

# Journal of Materials Chemistry C

Accepted Manuscript



This is an *Accepted Manuscript*, which has been through the Royal Society of Chemistry peer review process and has been accepted for publication.

*Accepted Manuscripts* are published online shortly after acceptance, before technical editing, formatting and proof reading. Using this free service, authors can make their results available to the community, in citable form, before we publish the edited article. We will replace this *Accepted Manuscript* with the edited and formatted *Advance Article* as soon as it is available.

You can find more information about *Accepted Manuscripts* in the [Information for Authors](#).

Please note that technical editing may introduce minor changes to the text and/or graphics, which may alter content. The journal's standard [Terms & Conditions](#) and the [Ethical guidelines](#) still apply. In no event shall the Royal Society of Chemistry be held responsible for any errors or omissions in this *Accepted Manuscript* or any consequences arising from the use of any information it contains.

# Thermometry and Optical Heating Bi-functional Properties of Upconversion Phosphor $\text{Ba}_5\text{Gd}_8\text{Zn}_4\text{O}_{21}:\text{Yb}^{3+}/\text{Tm}^{3+}$

Hao Suo<sup>a</sup>, Chongfeng Guo<sup>a\*</sup>, Zheng Yang<sup>a</sup>, Shaoshui Zhou<sup>b</sup>, Changkui Duan<sup>b</sup>, Min Yin<sup>b</sup>

a. National Key Laboratory of Photoelectric Technology and Functional Materials (Culture Base) in Shaanxi Province, National Photoelectric Technology and Functional Materials & Application of Science and Technology International Cooperation Base, Institute of Photonics & Photon-Technology, Northwest University, Xi'an, 710069, China;

b. School of Physical Science, University of Science and Technology of China, Hefei, 230026, China;

-----  
Author to whom correspondence should be addressed

E-mail: [guocf@nwu.edu.cn](mailto:guocf@nwu.edu.cn) (Prof. Guo);

Tel & Fax: ±86-29-88302661

## Abstract

$\text{Yb}^{3+}/\text{Tm}^{3+}$  co-doped  $\text{Ba}_5\text{Gd}_8\text{Zn}_4\text{O}_{21}$  *up-conversion (UC)* phosphors with thermometry and optical *heating* properties were *successfully* prepared by a sol-gel *process*, *crystal* structures of all samples were examined by X-ray diffraction (XRD). *The phosphors show an intense near-infrared (NIR) and several weak visible emission peaks* with 980 nm excitation. The possible UC mechanisms and processes were proposed based on the power dependence of *up-conversion luminescence (UCL)* intensities, and the lifetimes of  ${}^1\text{G}_4 \rightarrow {}^3\text{H}_6$  *blue emissions* were also *measured* to confirm the *occurrence* of energy transfer (ET). Temperature sensing performances based on the stark levels ( ${}^1\text{G}_{4(1)}$ ,  ${}^1\text{G}_{4(2)}$ ) of  $\text{Tm}^{3+}$  *were* evaluated by analyzing *temperature-dependent* UCL spectra in the range of 300-510 K. The maximum sensitivity for phosphors with different UCL intensity was discussed in detail and approached to approximately  $0.0061 \text{ K}^{-1}$  at 300K. Furthermore, *the heating property* produced by laser excitation was *also* measured, which caused temperature of sample *rising* from 278.8 to 321.8 K as increasing pump power from 638 to 1802 mW. Results indicate that  $\text{Yb}^{3+}/\text{Tm}^{3+}$  co-doped  $\text{Ba}_5\text{Gd}_8\text{Zn}_4\text{O}_{21}$  phosphors could be considered as potential candidates for temperature sensor and optical heater.

**Keywords:** Up-conversion; Thermometry; Optical heater.

## 1. Introduction

As one of fundamental physical parameters, the accurate measurement of temperature is crucial in scientific research and industrial production. Among the methods to determine temperature, the non-contact temperature sensing based on rare earth (RE) ions activated luminescent material has aroused considerable interests owing to their excellent accuracy and resolution in comparison with conventional temperature *detecting* devices using the principle of liquid and metal expansion because it is independent of spectrum losses and fluctuations in the excitation intensity [1-4]. Especially the optical thermometry based on the fluorescence intensity ratio (FIR) technology has been paid more attention due to its potential applications in electrical power stations, oil refineries and intracellular temperature, which takes advantage of the temperature-dependent up-conversion luminescence (UCL) intensities from two thermally coupled energy levels (TCLs) of RE ions. TCLs are closely spaced and assumed to be thermodynamically quasi equilibrium and the energy separation  $\Delta E$  between them generally ranging from  $200\text{ cm}^{-1}$  to  $2000\text{ cm}^{-1}$  to avoid strong overlapping of the two emissions and enable the upper level to have a minimum population of optically active ions in the interested temperature range [5]. Among rare earth ions, TCLs can be found in  $\text{Er}^{3+}$  ( $^4\text{S}_{3/2}$ ,  $^4\text{F}_{9/2}$ ),  $\text{Ho}^{3+}$  ( $^5\text{F}_{2,3}$ ,  $^3\text{K}_8$ ,  $^5\text{G}_6$ ,  $^4\text{F}_1$ ),  $\text{Nd}^{3+}$  ( $^4\text{F}_{7/2}$ ,  $^4\text{F}_{3/2}$ ;  $^4\text{F}_{5/2}$ ,  $^4\text{F}_{3/2}$ ;  $^4\text{F}_{7/2}$ ,  $^4\text{F}_{5/2}$ ),  $\text{Dy}^{3+}$  ( $^4\text{F}_{9/2}$ ,  $^4\text{I}_{15/2}$ ) and  $\text{Tm}^{3+}$  ( $^3\text{F}_{2,3}$ ,  $^3\text{H}_4$ ), *etc* [6-10]. However, these ions have weak and narrow absorption cross-sections and leading to low UC efficiency and high pumping power, resulting in considerable margin of errors for the sensor. In order to *solve* this problem,  $\text{Yb}^{3+}$  ion is introduced as an efficient sensitizer owing to its high absorption cross-section near 980 nm, which is also *beneficial* to reduce errors of sensor [11]. According to previous publications, the energy gap between  $^1\text{G}_{4(1)}$  and  $^1\text{G}_{4(2)}$  levels of  $\text{Tm}^{3+}$  is about  $315\text{ cm}^{-1}$ , which means that they can be selected as thermal coupled energy *levels and* used in optical thermometry. Up to now, only few researches reported temperature sensing UCL materials based on closely spaced stark levels ( $^1\text{G}_{4(1)}$ ,  $^1\text{G}_{4(2)}$ ) of  $\text{Tm}^{3+}$  ions [12, 13]. Owing to excellent physical and thermal stability, low phonon energy ( $360\text{ cm}^{-1}$ ), zincate complex oxide  $\text{Ba}_5\text{Gd}_8\text{Zn}_4\text{O}_{21}$  is regarded as an ideal potential matrix candidate for optical temperature sensing [14].

For the UC materials, part of energy absorbed was converted into internal heat through non-radiative channels, which is ordinarily considered as a main reason for low UCL efficiency

[15]. However, the laser induced heat generated by UCL materials has great potential in photo-thermal therapy (PTT) in which cancerous cells could be ablated by the heat transferred from incident energy [16]. In this process, the commercialized NIR laser commonly used as efficient excitation source thanks to its advantages of large penetration depth and no critical damage on tissues [17]. Thus, proper UCL materials could be served as optical heater and optically temperature sensor which could not only transfer the photon energy into the heat but also accurately measure the temperature in the procedure of photo-thermal therapy [18].

In this paper,  $\text{Yb}^{3+}$  sensitized  $\text{Tm}^{3+}$  doped  $\text{Ba}_5\text{Gd}_8\text{Zn}_4\text{O}_{21}$  UC phosphors were synthesized by sol-gel process and their UCL properties were *also* studied in detail. *Optical* temperature sensing property based on FIR method of phosphors with different  $\text{Yb}^{3+}$  contents were discussed by analyzing temperature-dependence UCL spectra. Moreover, the potential application for optical heater of samples was also investigated by monitoring the internal heat under different 980 nm laser pump power.

## 2. Experimental

### 2.1 Preparation of $\text{Ba}_5\text{Gd}_8\text{Zn}_4\text{O}_{21}:\text{Yb}^{3+}, \text{Tm}^{3+}$ phosphors.

The  $\text{Yb}^{3+}$  sensitized  $\text{Tm}^{3+}$  doped  $\text{Ba}_5\text{Gd}_8\text{Zn}_4\text{O}_{21}$  phosphors with chemical formula  $\text{Ba}_5\text{Gd}_8\text{Zn}_4\text{O}_{21}:x\text{Tm}^{3+}, y\text{Yb}^{3+}$  ( $x = 0\text{-}20\%$  and  $y = 0\text{-}1\%$ ) were synthesized through a citric acid chelating sol-gel process. Owing to the identical valence and similar ionic radius,  $\text{Yb}^{3+}$  and  $\text{Er}^{3+}$  ions are expected to occupy the sites of  $\text{Gd}^{3+}$ . In the typical experimental procedure, stoichiometric amounts of rare earth oxides with high purity  $\text{Ln}_2\text{O}_3$  ( $\text{Ln} = \text{Yb}, \text{Tm}, \text{Gd}$ ; 99.99%, Shanghai Yuelong Nonferrous Metals Ltd.) were first dissolved in  $\text{HNO}_3$  (A.R.) solution to get rare earth nitrate ( $\text{Ln} = \text{Yb}, \text{Tm}, \text{Gd}$ ) and excessive nitric acid were volatilized by evaporation, then suitable amount of deionized water was added with constant stirring to form transparent solution. Subsequently, the calculated quantity of citric acid (molar ratio of citric acid to total metal ions was 2:1) was introduced into the above solution acting as chelating agent. Then the required analytical grade  $\text{BaCO}_3$  and  $\text{ZnO}$  were dissolved in obtained solution under vigorous stirring. After continuous stirring for a few minutes, the obtained transparent aqueous solution was kept in an oven at 80 °C to get colorless transparent resin and further dried at 120 °C for 24 h to

obtain brown dried gel. Finally, the samples were formed by sintering at 1200 °C for 3 h after preheating the dried gel at 500 °C for 5 h.

## 2.2 Measurements and characterization

The characterization of crystalline phase and structure were identified by XRD in the range of  $10^\circ \leq 2\theta \leq 60^\circ$  performed on a Rigaku-Dmax 3C powder diffractometer (Rigaku Corp, Tokyo, Japan) with Cu-K $\alpha$  ( $\lambda = 1.54056 \text{ \AA}$ ) radiation. The UCL properties of phosphors at room temperature (RT) were recorded on a FLS920 fluorescence spectrophotometer equipped with an external power-controllable 980 nm semiconductor laser as excitation source. The measurement of lifetime for  $^1G_4 \rightarrow ^3H_6$  transitions of Tm $^{3+}$  at room temperature were carried out using 980 nm pulsed laser of an optical parametric oscillator (OPO) as excitation source, and the signals were analyzed by a Tektronix digital oscilloscope (TDS 3052). The UCL spectra of samples at various temperatures from RT to 240 °C were obtained using a Jobin-Yvon HRD-1 double monochromator with a Hamamatsu R928 Photomultiplier under the 980 nm excitation with the pump power of 28.5 mW and the signal was detected by an EG&G 7265 DSP Lock-in Amplifier.

## 3. Results and discussion

### 3.1 X-ray diffraction analysis

To investigate the crystal structure and phase purity, Tm $^{3+}$  single-doped and Tm $^{3+}$ -Yb $^{3+}$  co-doped Ba $_5$ Gd $_8$ Zn $_4$ O $_{21}$  phosphors with different dopant concentrations were characterized by XRD. All samples obtained in our experiments show similar results, the XRD patterns of Ba $_5$ Gd $_8$ Zn $_4$ O $_{21}$  ( $x = 0, y = 0.3\%; x = 10\%, y = 0.3\%, 0.5\%, 0.7\%$ , and 1%) were presented in Fig. 1(a) as representatives. All the observed diffraction peaks of the phosphors can be perfectly indexed to the tetragonal phase of Ba $_5$ Gd $_8$ Zn $_4$ O $_{21}$  (JCPDS No. 51-1686) and no other diffraction peaks from any impurity were found. With the increase of dopant concentrations, it is observed that the positions of the diffraction peaks of the sample gradually shift to large angles (as shown the enlarged (321) peaks in Fig. 1(b)) due to the smaller radius of Yb $^{3+}$  (0.86Å) and Tm $^{3+}$  (0.87Å) than that of Gd $^{3+}$  (0.94Å), leading to the shrinking of the unit cell volume (as shown Table S1). Above results reveals that the Tm $^{3+}$  or Yb $^{3+}$  ions have effectively incorporated into host lattices by replacing Gd $^{3+}$  sites.

### 3.2 Spectra of Ba<sub>5</sub>Gd<sub>8</sub>Zn<sub>4</sub>O<sub>21</sub>: Yb<sup>3+</sup>, Tm<sup>3+</sup> phosphors at RT

The UC emission spectra of as-synthesized Ba<sub>5</sub>Gd<sub>8</sub>Zn<sub>4</sub>O<sub>21</sub>: 0.3%Tm<sup>3+</sup>, 11%Yb<sup>3+</sup> phosphors at room temperature upon the excitation of 980 nm laser diodes in the wavelength range of 430-870 nm are displayed in Fig. 2(a). It is clearly observed that the obtained UCL *spectrum* of Tm<sup>3+</sup>/Yb<sup>3+</sup> codoped Ba<sub>5</sub>Gd<sub>8</sub>Zn<sub>4</sub>O<sub>21</sub> is composed of an intense NIR emission and several relatively weak peaks in visible region. The former emission peak centered at 798 nm is originated from <sup>3</sup>H<sub>4</sub> → <sup>3</sup>H<sub>6</sub> transition of Tm<sup>3+</sup>, while the latter weak emission lines are assigned to <sup>1</sup>G<sub>4(2)</sub> → <sup>3</sup>H<sub>6</sub> (479 nm), <sup>1</sup>G<sub>4(1)</sub> → <sup>3</sup>H<sub>6</sub> (484 nm), <sup>1</sup>G<sub>4</sub> → <sup>3</sup>F<sub>4</sub> (654 nm) and <sup>3</sup>F<sub>2,3</sub> → <sup>3</sup>H<sub>6</sub> (695 nm) intrinsic transitions of Tm<sup>3+</sup> ions, respectively. Interestingly, it is found that the blue emission band was divided into two sections due to the impact of spin-orbit coupling and interactions among electrons, which leads to the emergence of stark sublevels <sup>1</sup>G<sub>4(1)</sub> and <sup>1</sup>G<sub>4(2)</sub> [19]. However, the emission in green region appeared though no corresponding energy level transitions from Tm<sup>3+</sup> are attributed, which has been found in previous publications and maybe assigned to <sup>5</sup>F<sub>4</sub>/<sup>5</sup>S<sub>2</sub> → <sup>5</sup>I<sub>8</sub> of impurity Ho<sup>3+</sup> ion from raw materials [20, 21]. The dopant concentrations greatly influence the photoluminescence intensity, thus the dependence of integrated UCL intensity of Ba<sub>5</sub>Gd<sub>8(1-x-y)</sub>Yb<sub>8x</sub>Tm<sub>8y</sub>Zn<sub>4</sub>O<sub>21</sub> upon the contents of Tm<sup>3+</sup> and Yb<sup>3+</sup> were investigated and shown in Fig (b) and (c). It is found that the optimum concentrations of Yb<sup>3+</sup> and Tm<sup>3+</sup> are determined to be 11% and 0.3%, then UCL intensity sharply drop with further increasing dopants contents due to the concentration quenching [22]. Both blue emission and NIR emission intensity are also dependent on the contents of Tm<sup>3+</sup> and Yb<sup>3+</sup>, and show similar variation trend to that of total UCL intensity, as shown in Fig.S1.

### 3.3 Energy level diagram and pump power dependence study

In order to comprehend the UC mechanism and UC processes, the double logarithmic plots of the emission intensity  $I_{f-f}$  as a function of pump power  $P_{980}$  and possible UC processes are depicted in Fig.3(a) and (b), respectively. It is generally accepted that multiple phonons were involved in the UC process, and the number of the NIR photons ( $n$ ) absorbed per up-converted photon emitted could be determined according to the relation between UCL intensity ( $I$ ) and the pump power ( $P$ ):  $I \propto P^n$  [23]. The values of  $n$  is obtained from the slope of the straight line by fitting the log-log plot of visible and NIR emission integrated intensities as variables of excitation power. As demonstrated in Fig. 3(a), the obtained  $n$  values were 2.96, 2.45, 1.82 and 1.49 for blue (484 nm), red (654, 695 nm) and NIR (798 nm) emissions, which indicates that the red emission centered at

654 nm and blue emission are assigned to three-photon absorption process whereas the red emission peaked at 695 nm and NIR emission are populated by two-photon absorption process.

According to above results, the possible UC processes are schematically given in the energy level diagrams of  $\text{Tm}^{3+}$  and  $\text{Yb}^{3+}$  and feasible transitions were also displayed in Fig. 3(b). Under the excitation of 980 nm laser, an NIR photon is absorbed by  $\text{Yb}^{3+}$  ion leading to the transition of  ${}^2\text{F}_{2/7} \rightarrow {}^2\text{F}_{2/5}$ . For the population  ${}^3\text{F}_4$  level of  $\text{Tm}^{3+}$  is realized by non-radiative (NR) relaxation from the upper  ${}^3\text{H}_5$  level which is populated through ET process:  $\text{Tm}^{3+} ({}^3\text{H}_6) + \text{Yb}^{3+} ({}^2\text{F}_{2/5}) \rightarrow \text{Tm}^{3+} ({}^3\text{H}_5) + \text{Yb}^{3+} ({}^2\text{F}_{2/7})$  or ground state absorption (GSA) process:  ${}^3\text{H}_6 \rightarrow {}^3\text{H}_5$ . After exciting population of  ${}^3\text{F}_4$  state to higher  ${}^3\text{F}_{2,3}$  states by ET process or excited state absorption (ESA) process:  $\text{Tm}^{3+} ({}^3\text{F}_4) + h\nu \rightarrow \text{Tm}^{3+} ({}^3\text{F}_{2,3})$ , the non-radiative relaxation from  ${}^3\text{F}_{2,3}$  to  ${}^3\text{H}_4$  level take place. As a result of ET process:  $\text{Tm}^{3+} ({}^3\text{H}_4) + \text{Yb}^{3+} ({}^2\text{F}_{2/5}) \rightarrow \text{Tm}^{3+} ({}^1\text{G}_4) + \text{Yb}^{3+} ({}^2\text{F}_{2/7})$ , the stark sublevels  ${}^1\text{G}_{4(1)}$  and  ${}^1\text{G}_{4(2)}$  of  ${}^1\text{G}_4$  state are populated via radiative relaxation to the ground state and produce two blue emissions at 484 and 479 nm, respectively. The population at  ${}^1\text{G}_4$  state relaxed rapidly to  ${}^3\text{F}_4$  level and radiative relaxation from  ${}^3\text{F}_{2,3}$  levels to ground state  ${}^3\text{H}_6$  generate red emission around 654 and 695 nm, respectively. After NR process taking place from  ${}^3\text{F}_{2,3}$  to lower  ${}^3\text{H}_4$  level, the population at  ${}^3\text{H}_4$  level decays radiatively to ground state with NIR emission at 798 nm.

### 3.4 Lifetime measurements

According to above analysis on UC mechanism and possible UC processes, it can be concluded that the efficient ET from  $\text{Yb}^{3+}$  to  $\text{Tm}^{3+}$  ions plays a crucial role in enhancing UC intensities. Generally, a rise time at initial stage may be observed in the UC luminescence decay for an energy transfer upconversion (ETU) process, since the population of the UC luminescent level requires an ET between two ions, whereas such a rise time does not appear in GSA and ESA. To further confirm and understand the influence of the ET from  $\text{Yb}^{3+}$  to  $\text{Tm}^{3+}$  on the UCL, the UC luminescence decays of the  ${}^1\text{G}_4 \rightarrow {}^3\text{H}_6$  emission in  $\text{Ba}_5\text{Gd}_8\text{Zn}_4\text{O}_{21}: 0.3\%\text{Tm}^{3+}, x\text{Yb}^{3+}$  ( $x = 0, 11\%$ ) were measured upon the excitation of 980 nm pulsed laser at room temperature. As shown in Fig. 4, it can be observed that an initial rise in the UCL decay for  $\text{Yb}^{3+}\text{-Tm}^{3+}$  co-doped phosphors, resulting from  $\text{Yb}^{3+} \rightarrow \text{Tm}^{3+}$  ET process that involves the intermediate level (e. g.  ${}^2\text{F}_{2/5}$  of  $\text{Yb}^{3+}$ ) with a rather long PL lifetime. Therefore, it can conclude that the ET process may be the primary process for the present UC emission [23]. In sharp contrast, such an initial rise time was not

observed in  $Tm^{3+}$  singly doped counterparts, suggesting that UC emissions in  $Ba_5Gd_8Zn_4O_{21}: 0.3\%Tm^{3+}$  occur mainly through the ESA/GSA processes. The effective lifetime of the blue level could be calculated by equation (1) [24]:

$$\tau = \frac{\int_0^{\infty} I(t)tdt}{\int_0^{\infty} I(t)dt} \quad (1)$$

Where  $I(t)$  represents the UCL intensity at time  $t$ . The decay profile can be well fitted with quadratic exponential function and the average lifetime can be computed using following equation (2) [25]:

$$\bar{\tau} = \frac{A_1t_1^2 + A_2t_2^2}{A_1t_1 + A_2t_2} \quad (2)$$

As displayed in Fig.4, the lifetime of blue  ${}^1G_4 \rightarrow {}^3H_6$  emission in co-doped sample  $Ba_5Gd_8Zn_4O_{21}: 0.3\%Tm^{3+}, 11\%Yb^{3+}$  ( $90 \mu s$ ) is larger than that of in  $Ba_5Gd_8Zn_4O_{21}: 0.3\%Tm^{3+}$  ( $40 \mu s$ ), which also proves the existence of the ET processes from  $Yb^{3+}$  to  $Tm^{3+}$  ions. *As a matter of fact, the observed UCL lifetime may to some extent reflect the decay nature of the intermediate states in the UC process [26].*

### 3.5 Optical temperature sensing behavior

In terms of the FIR based optical thermometry technique, it is a sticking point to select two appropriate thermal coupling levels (TCL) from rare earth ions and investigate their corresponding UCL intensity ratio varying with temperature. In order to find out whether the stark sublevels  ${}^1G_{4(1)}$  and  ${}^1G_{4(2)}$  of  $Tm^{3+}$  are thermally coupled or not, the temperature dependence of UCL spectra (300-510 K) for  $Ba_5Gd_8Zn_4O_{21}: 0.3\%Tm^{3+}, 11\%Yb^{3+}$  in blue region were illuminated in Fig. 5 with 980 nm NIR laser excited. It is worth noted that the excitation power is too low (28.5 mW) to generate thermal effect caused by pump laser, which ensured the accuracy of obtained experimental results. As shown in Fig. 5, it clearly observed that the intensity of entire blue emission spectra decreased sharply with the increase of temperature, whereas the FIR ( $I_{479}/I_{484}$ ) of two blue emission bands varied greatly with unchanged band positions. Owing to the effective non-radiative process between closely spaced stark sublevels, the  ${}^1G_{4(2)}$  level could be populated by thermal excitation from  ${}^1G_{4(1)}$  level [27]. Therefore, it can be inferred that the stark sublevels  ${}^1G_{4(1)}$  and  ${}^1G_{4(2)}$  of  $Tm^{3+}$  can be regarded as TCLs and relative population of which follows the

Boltzmann distribution. The FIR of the emissions from  ${}^1G_{4(2)}$ ,  ${}^1G_{4(1)} \rightarrow {}^3H_6$  could be mathematically written as [28]:

$$R = \frac{I_{479}}{I_{484}} = \frac{N({}^1G_{4(2)})}{N({}^1G_{4(1)})} = \frac{g_2 \sigma_2 \omega_2}{g_1 \sigma_1 \omega_1} \exp\left(-\frac{\Delta E}{KT}\right) = C \exp\left(-\frac{\Delta E}{KT}\right) \quad (3)$$

where  $I_{479}$  and  $I_{484}$  denote the integrated intensities of  ${}^1G_{4(2)} \rightarrow {}^3H_6$  and  ${}^1G_{4(1)} \rightarrow {}^3H_6$  transitions, respectively.  $N({}^1G_{4(2)})$  and  $N({}^1G_{4(1)})$  represent the population of corresponding energy level while the degeneracy, emission cross-section and angular frequency of corresponding transitions are symbolized by  $g$ ,  $\sigma$  and  $\omega$ .  $\Delta E$  is the energy separation between stark sublevels,  $T$  is absolute temperature,  $K$  is Boltzmann constant and  $C$  is the proportionality factor ( $C = g_2 \sigma_2 \omega_2 / g_1 \sigma_1 \omega_1$ ). The monolog of FIR ( $\ln FIR$ ) as a function of inverse absolute temperature ( $1/T$ ) for  $Ba_5Gd_8Zn_4O_{21}: 0.3\%Tm^{3+}, 11\%Yb^{3+}$  phosphor is displayed in the inset of Fig.5, in which the experimental FIR results are perfectly fitted by a straight line with a slope of about 491.6. This slope practically gives the value of  $\Delta E/K$  and the calculated energy gap  $\Delta E$  between two stark sublevels  ${}^1G_{4(1)}$  and  ${}^1G_{4(2)}$  is about  $342 \text{ cm}^{-1}$ .

Fig.6 illustrates the variation of FIR and relative sensitivity with absolute temperature, in which the FIR increased from 1.1 to 2.2 as temperature raising from 300 to 510 K. The obtained value of coefficient  $C$  comes out to be about 5.698 according to the best fit curve on experimental data. As for relative sensitivity, it is a prominent parameter to quantitatively determine an optical sensor whether or not *be favorable to* application and defined as the theoretical rate of the FIR changing with temperature and can be written as [29]:

$$S = \frac{dR}{dT} = R\left(\frac{\Delta E}{KT^2}\right) = C\left(\frac{R}{T^2}\right) \quad (4)$$

The corresponding curve of relative sensitivity varying with temperature is also presented in Fig. 6. It can be clearly observed that the value of relative sensitivity is about  $0.0061 \text{ K}^{-1}$  at 300 K and keep dropping with increase of temperature in our experimental range, which shows similar trend with previous literatures. The present sensitivity achieved in  $Yb^{3+}/Tm^{3+}$  co-doped  $Ba_5Gd_8Zn_4O_{21}$  phosphors as optically temperature sensors is higher than that of  $Y_2O_3$  ( $0.0035 \text{ K}^{-1}$ ),  $NaNbO_3$  ( $0.08\% \text{ C}^{-1}$ ) and  $Na_2Y_2B_2O_7$  ( $0.0045 \text{ K}^{-1}$ ) using stark levels of  ${}^1G_4$  as TCL [12, 13, 30].

As well-known, many factors may exert effects on relative sensitivity of optical temperature sensors, such as host material, particle size, UC intensity and so on [31]. To figure out the effect of

UCL intensity (or dopant concentrations) on sensor sensitivity, the optical thermometry performance of Yb<sup>3+</sup>/Tm<sup>3+</sup> co-doped Ba<sub>5</sub>Gd<sub>8</sub>Zn<sub>4</sub>O<sub>21</sub> phosphors with different Yb<sup>3+</sup> concentrations were investigated in detail, as shown in Fig. 7. The energy gap  $\Delta E$  of stark sublevels <sup>1</sup>G<sub>4(1)</sub> and <sup>1</sup>G<sub>4(2)</sub> in Ba<sub>5</sub>Gd<sub>8</sub>Zn<sub>4</sub>O<sub>21</sub>: 0.3%Tm<sup>3+</sup>, 15%Yb<sup>3+</sup> and Ba<sub>5</sub>Gd<sub>8</sub>Zn<sub>4</sub>O<sub>21</sub>: 0.3%Tm<sup>3+</sup>, 20%Yb<sup>3+</sup> phosphors can be calculated to be about 336 and 355 cm<sup>-1</sup>, the corresponding values of coefficient  $C$  are 5.584 and 5.930, respectively. Furthermore, the obtained relative sensitivities of two samples reach the maximum 0.0062 K<sup>-1</sup> and 0.0063 K<sup>-1</sup> at 300 K then decrease sharply as increasing temperature, which are in close agreement with the results of Ba<sub>5</sub>Gd<sub>8</sub>Zn<sub>4</sub>O<sub>21</sub>: 0.3%Tm<sup>3+</sup>, 11%Yb<sup>3+</sup>. Although the UC emission intensities are significantly different (*shown in Fig 2(c)*), three mentioned phosphors exhibit similar optical thermometry behaviors within the error range, indicating UCL intensity hardly influence sensitivity of optical temperature sensor.

### 3.6 Optical heater based analysis

In order to investigate the effects of *laser* induced thermal effect, blue UC emission spectra of samples from 638 to 1802 mW and the *plots* of the calculated FIR of <sup>1</sup>G<sub>4(1)</sub>, <sup>1</sup>G<sub>4(2)</sub> → <sup>3</sup>H<sub>6</sub> transitions as a function of pump power are displayed in Fig.8. It can be found that the value of FIR raise from 0.97 to 1.23 with increasing the pump power from 638 to 1802 mW. According to the optical temperature sensing properties mentioned above, the given value of FIR represents a particular temperature, so the *host* temperature heated by laser excitation at different pump power can be easily calculated by following equation (5) which is rearranged from equation (3) [32]:

$$T = \left[ \frac{1}{\ln(C) - \ln\left(\frac{I_{479}}{I_{484}}\right)} \right] \left( \frac{\Delta E}{K} \right) \quad (5)$$

where all the terms have their usual implications as mentioned *eq.* (3). The plot of the calculated lattice temperature using equation (5) is also depicted in the inset as a function of pump power, in which the lattice temperature varies from 278.8 to 321.8 K with the increase of pump power from 638 to 1802 mW. In general, the phonon-assisted non-radiative relaxation process and crystalline property of phosphors are primary reasons why materials can generate heat under the laser excitation. In addition, interaction between electron and phonon could be improved by the effect of quantum confinement among phonons, which results the internal heat generation in crystalline phosphors [18]. Due to the capability of transferring laser excitation power into heat, Yb<sup>3+</sup>-Tm<sup>3+</sup>

co-doped  $\text{Ba}_5\text{Gd}_8\text{Zn}_4\text{O}_{21}$  phosphors have also great potential of acting as an optical heater used in photo-thermal therapy.

#### 4. Conclusion

A series of  $\text{Yb}^{3+}$  and  $\text{Tm}^{3+}$  doped  $\text{Ba}_5\text{Gd}_8\text{Zn}_4\text{O}_{21}$  phosphors with various dopant contents were prepared by a sol-gel method. Pumped by 980 nm, an intense emission in NIR region peaked at 798 nm from  $^3\text{H}_4 \rightarrow ^3\text{H}_6$  transition and several weak visible emission bands from  $^1\text{G}_{4(2)} \rightarrow ^3\text{H}_6$  (479 nm),  $^1\text{G}_{4(1)} \rightarrow ^3\text{H}_6$  (484 nm),  $^1\text{G}_4 \rightarrow ^3\text{F}_4$  (654 nm) and  $^3\text{F}_{2,3} \rightarrow ^3\text{H}_6$  (695 nm) intrinsic transitions of  $\text{Tm}^{3+}$  ions were observed in UCL spectra of phosphors. The UC mechanisms and possible UC processes were proposed, in which ET plays a dominant role. The decay time of the  $^1\text{G}_4 \rightarrow ^3\text{H}_6$  emissions were also measured to prove the presence of ET process. The FIR of blue UC emission peaked at 479 and 484 nm from two thermal coupling energy levels  $^1\text{G}_{4(2)}/^1\text{G}_{4(1)} \rightarrow ^3\text{H}_6$  was recorded in the temperature range of 300 - 510 K and the maximum sensitivity of phosphors with optimal dopant concentration is about  $0.0061 \text{ K}^{-1}$  at 300 K. The sensitivity is hardly influenced by UCL intensity for the phosphors with different  $\text{Yb}^{3+}$  contents. Moreover, laser induced thermal effect was also investigated and the sample lattice temperature varied from 278.8 to 321.8 K with increasing the pump power from 638 to 1802 mW. Results indicated that the present UC phosphors  $\text{Ba}_5\text{Gd}_8\text{Zn}_4\text{O}_{21}:\text{Tm}^{3+}, \text{Yb}^{3+}$  are ideal candidates for optically thermometer and optical heater.

#### Acknowledgements

This work was supported by the high-level talent project of Northwest University, National Natural Science Foundation of China (No. 11274251, 11274299, 11374291), Research Fund for the Doctoral Program of Higher Education of China (RFDP) (No.20136101110017), Technology Foundation for Selected Overseas Chinese Scholar, Ministry of Personnel of China (excellent), Natural Science Foundation of Shaanxi Province (No.2014JM1004) and Foundation of Key Laboratory of Photoelectric Technology in Shaanxi Province (12JS094).

## References

- [1] L. H. Fischer, G. S. Harms and O. S. Wolfbeis, *Angew. Chem., Int. Ed.*, 2011, **50**, 4546-4551.
- [2] C. D. S. Brites, P. P. Lima, N. J. O. Silva, A. Mall'an, V. Amaral, F. Palacio and L. d. Carlos, *New J. Chem.*, 2011, **35**, 1177-1183.
- [3] J. M. Yang, H. Yang and L. Lin, *ACS Nano.*, 2011, **5**, 5067-5071.
- [4] A. Sedlmeier, D. E. Achatz, L. H. Fischer, H. H. Gorris and O. S. Wolfbeis, *Nanoscale*, 2012, **40**, 7090-7096.
- [5] L. Li, C. F. Guo, S. Jiang, D. K. Agrawal and T. Li, *RSC Adv.*, 2014, **4**, 6391-6396.
- [6] B. Dong, B. Cao, Y. He, Z. Liu, Z. Li and Z. Feng, *Adv. Mater.*, 2012, **24**, 1987-1993.
- [7] S. S. Zhou, S. Jiang, X. T. Wei, Y. H. Chen, C. K. Duan and M. Yin, *J. Alloy Compd.*, 2014, **588**, 654-657.
- [8] W. Xu, Q. T. Song, L. J. Zhang, Z. G. Zhang and W. W. Cao, *Opt. lett.*, 2014, **39**, 4635-4638.
- [9] S. A. Wade, S. F. Collins and G. W. Baxter, *J. Appl. Phys.*, 2003, **94**, 4743-4756.
- [10] L. L. Xing, Y. L. Xu, R. Wang, W. Xu and Z. G. Zhang, *Opt. lett.*, 2014, **39**, 454-457.
- [11] A. K. Soni and V. K. Rai, *Dalton Trans.*, 2014, **43**, 13563-13570.
- [12] D. Y. Li, Y. X. Wang, X. R. Zhang, K. Yang, L. Liu and Y. L. Song, *Opt. Commun.*, 2012, **285**, 1925-1928.
- [13] A. K. Soni, R. Dey and V. K. Rai, *RSC Adv.*, 2015, **5**, 34999-35009.
- [14] B. N. Tian, B. J. Chen, Y. Tian, X. P. Li, J. S. Zhang, J. S. Sun, H. Y. Zhong, L. H. Cheng, S. B. Fu, H. Zhong, Y. Z. Wang, X. Q. Zhang, H. P. Xia and R. N. Hua, *J. Mater. Chem. C*, 2013, **1**, 2338-2344.
- [15] Y.M. Yang, C. Mi, F. Yu, X. Y. Su, C. F. Guo, G. Li, J. Zhang, L. L. Liu, Y. Z. Liu and X. D. Li, *Ceram.Int.*, 2014, **40**, 9875-9880.
- [16] L. C. Kennedy, L. R. Bickford, N. A. Lewinski, A. J. Coughlin, Y. Hu, E. S. Day, J. L. West and R. A. Drezek, *Small.*, 2011, **7**, 169-183.
- [17] Y. F. Wang, G. Y. Liu, L. D. Sun, J. W. Xiao, J. C. Zhou and C. H. Yan, *ACS nano.*, 2013, **7**, 7200-7206.
- [18] R. Dey, A. Pandey and V. K. Rai, *Sens. Actuators, B*, 2014, **190**, 512-515.
- [19] A. Patra, P. Ghosh, P. S. Chowdhury, M. A. R. C. Alencar, W. Lozano, N. Rakov and G. S. Maciel, *J. Phys. Chem. B.*, 2005, **109**, 10142-10146.
- [20] G. Glaspell, J. Anderson, J.R. Wilkins and M. S. El-Shall, *J. Phys. Chem. C.*, 2008, **112**, 11527-11531.
- [21] T. Li, C. F. Guo, H. Jiao, L. Li and D. K. Agrawal, *Opt. Commun.*, 2014, **312**, 284-286.
- [22] L. Li, H. H. Lin, X. Q. Zhao, Y. J. Wang, X. J. Zhao, C. G. Ma and X. T. Wei, *J. Alloy Compd.*, 2014, **586**,

555-560.

[23] T. Li, C. F. Guo and L. Li, *Opt. Express*, 2013, **21**, 18281–18289.

[24] H. Jing, C. F. Guo, G. G. Zhang, X. Y. Su, Z. Yang and J. H. Jeong, *J. Mater. Chem.*, 2012, **22**, 13612–13618.

[25] T. Fujii, K. Kodaira, O. Kawauchi, N. Tanaka, H. Yamashita and M. Anpo, *J. Phys. Chem. B*, 1997, **101**, 10631–10637.

[26] W. Q. Luo, C. Y. Fu, R. F. Li, Y. S. Liu, H. M. Zhu and X. Y. Chen, *Small*, 2011, **7**: 3046-3056.

[27] V. K. Rai and S. B. Rai, *Spectrochim. Acta Part A*, 2007, **68**, 1406–1409

[28] A. K. Singh, S. K. Singh, B. K. Gupta, R. Prakash and S. B. Rai, *Dalton Trans.*, 2013, **42**, 1065-1072.

[29] K. Z. Zheng, Z. Y. Liu, C. J. Lv and W. P. Qin, *J. Mater. Chem. C.*, 2013, **1**, 5502–5507.

[30] A.F. Pereira, K. U. Kumar, W.F. Silva, W.Q. Santos, D. Jaque, C. Jacinto, *Sens. Actuators, B*, 2015, **213**, 65-71.

[31] B. Dong, R. N. Hua, B. S. Cao, Z. P. Li, Y. Y. He, Z. Y. Zhang and O. S. Wolfbeis, *Phys. Chem. Chem. Phys.*, 2014, **16**, 20009-20012.

[32] M. Challenor, P. J. Gong, D. Lorensen, M. Fitzgerald, S. Dunlop, D. D. Sampson and K. S. Iyer, *ACS Appl. Mater. Inter.*, 2013, **5**, 7875–7880.

## Figures

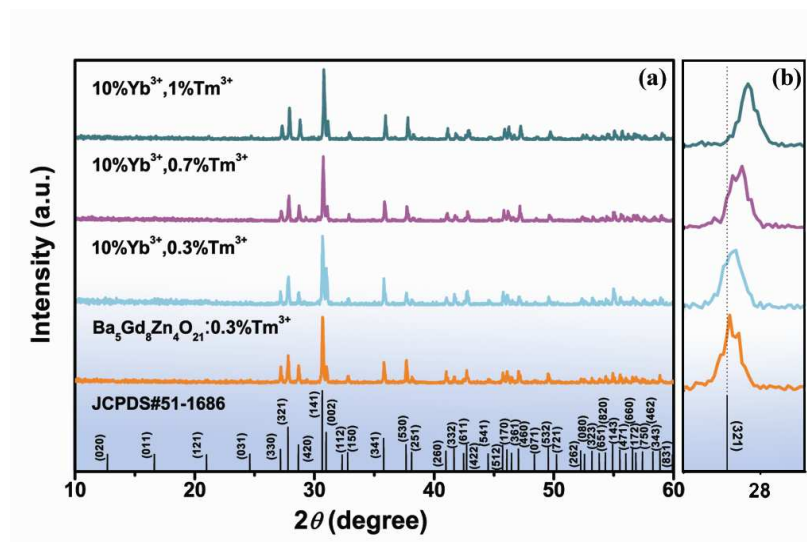


Fig. 1(a) XRD pattern of  $\text{Tm}^{3+}$  singly doped and  $\text{Tm}^{3+}$ - $\text{Yb}^{3+}$  co-doped as well as the standard profile of  $\text{Ba}_5\text{Gd}_8\text{Zn}_4\text{O}_{21}$ , (b) enlarged (321) peaks in various XRD patterns.

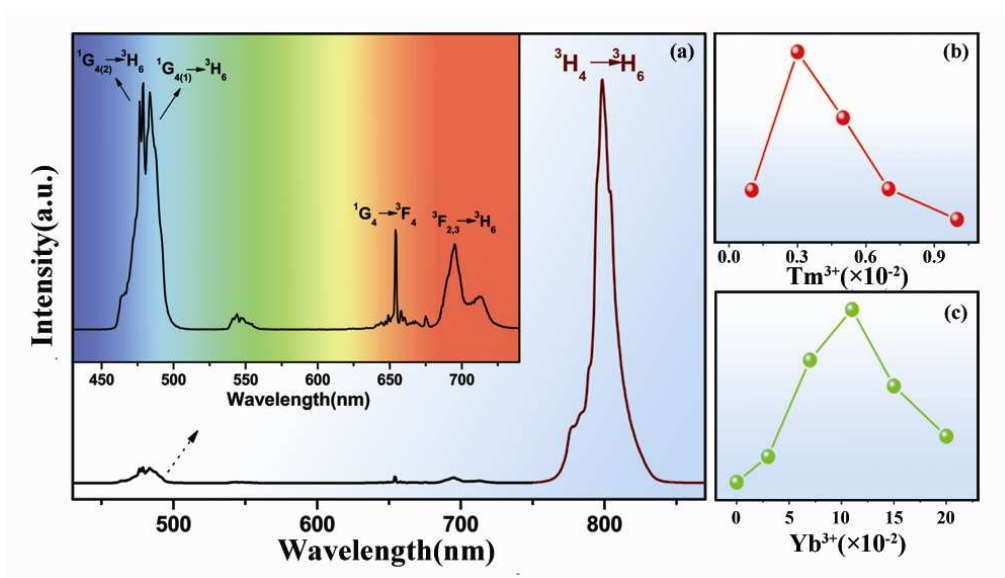


Fig. 2 UCL spectra of  $\text{Ba}_5\text{Gd}_8\text{Zn}_4\text{O}_{21}:0.3\% \text{Tm}^{3+}, 11\% \text{Yb}^{3+}$  under 980 nm excitation (a) and integrated UCL intensities as a function of  $\text{Tm}^{3+}$  concentrations ( $10\% \text{Yb}^{3+}$ ) (b),  $\text{Yb}^{3+}$  concentrations ( $0.3\% \text{Tm}^{3+}$ ) (c).

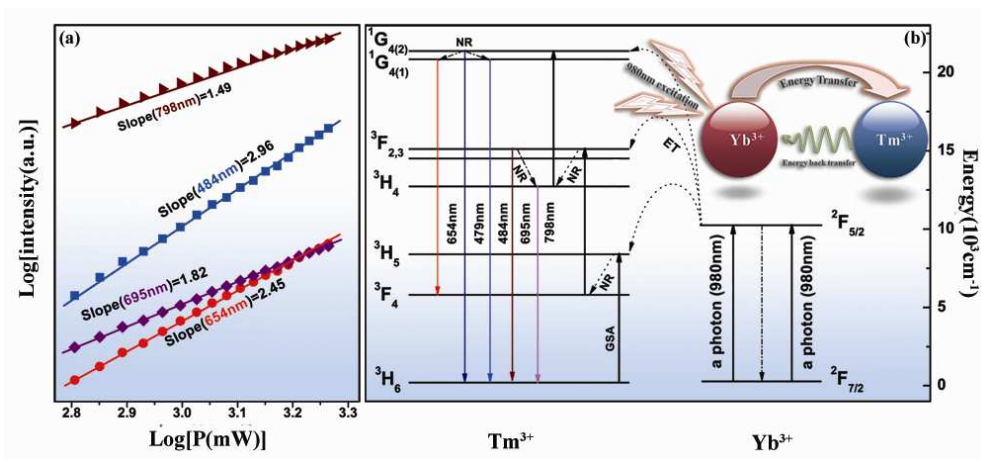


Fig. 3 (a) The double logarithmic plot of visible and NIR emission intensity versus excitation power in Ba<sub>5</sub>Gd<sub>8</sub>Zn<sub>4</sub>O<sub>21</sub>: 0.3%Tm<sup>3+</sup>, 11%Yb<sup>3+</sup>, (b) Simplified energy diagram for Yb<sup>3+</sup>, Tm<sup>3+</sup> ions along with the proposed UC processes.

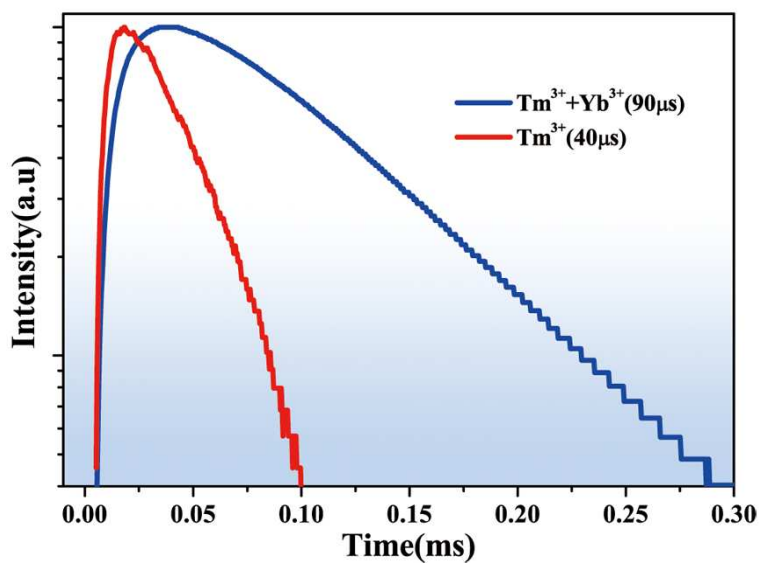


Fig. 4 The temporal evolution of <sup>1</sup>G<sub>4</sub> → <sup>3</sup>H<sub>6</sub> emission in Ba<sub>5</sub>Gd<sub>8</sub>Zn<sub>4</sub>O<sub>21</sub>: 0.3%Tm<sup>3+</sup>, xYb<sup>3+</sup> (x=0, 11%) after 980 nm pulsed laser excitation.

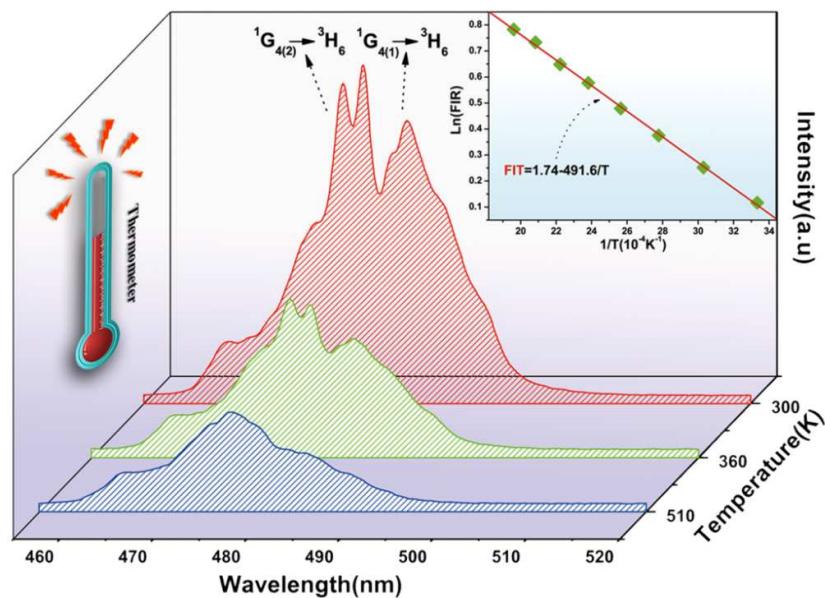


Fig. 5 NIR excited (980nm) thermal evolution blue UCL spectra of  $\text{Ba}_5\text{Gd}_8\text{Zn}_4\text{O}_{21}: 0.3\%\text{Tm}^{3+}, 11\%\text{Yb}^{3+}$  phosphors. Inset: the  $\ln(\text{FIR})$  as a function of inverse absolute temperature.

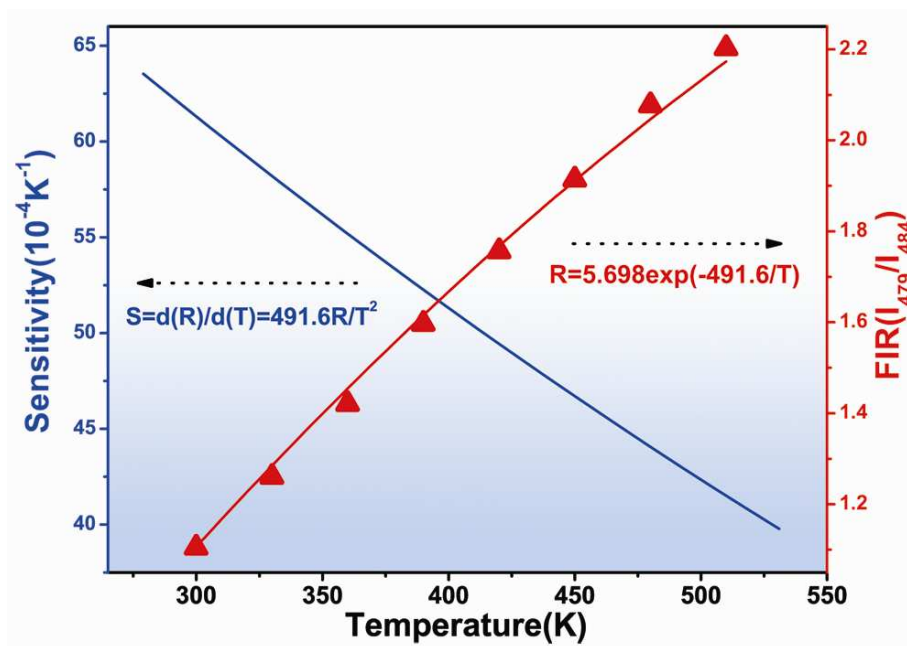


Fig.6 Dependence of relative sensitivity (blue) and FIR (red) of stark sublevels  $^1\text{G}_{4(1)}$  and  $^1\text{G}_{4(2)}$  upon the absolute temperature in range of 300- 510K for  $\text{Ba}_5\text{Gd}_8\text{Zn}_4\text{O}_{21}: 0.3\%\text{Tm}^{3+}, 11\%\text{Yb}^{3+}$  phosphor

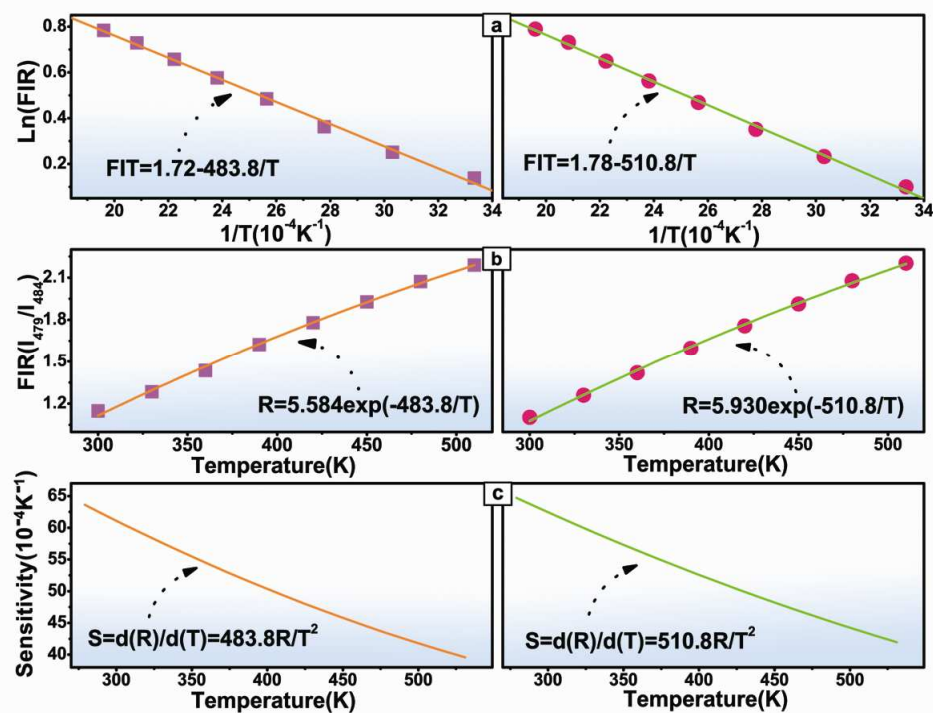


Fig. 7 Dependence of relative sensitivities upon temperature for  $\text{Ba}_5\text{Gd}_8\text{Zn}_4\text{O}_{21}: 0.3\%\text{Tm}^{3+}, 15\%\text{Yb}^{3+}$  (left) and  $\text{Ba}_5\text{Gd}_8\text{Zn}_4\text{O}_{21}: 0.3\%\text{Tm}^{3+}, 20\%\text{Yb}^{3+}$  (right)

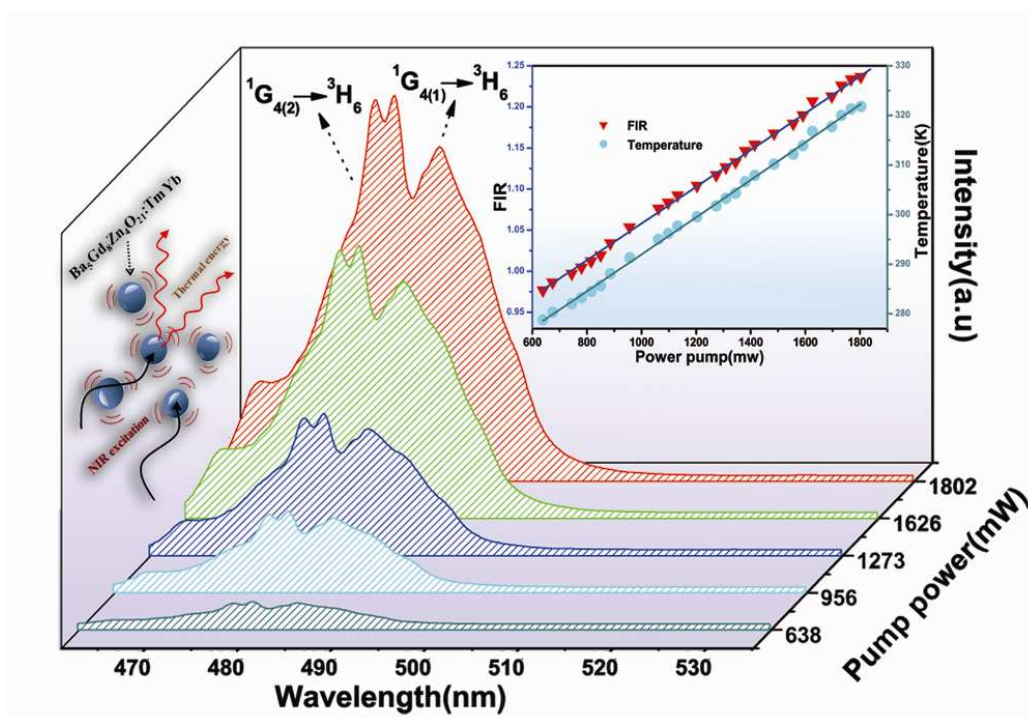
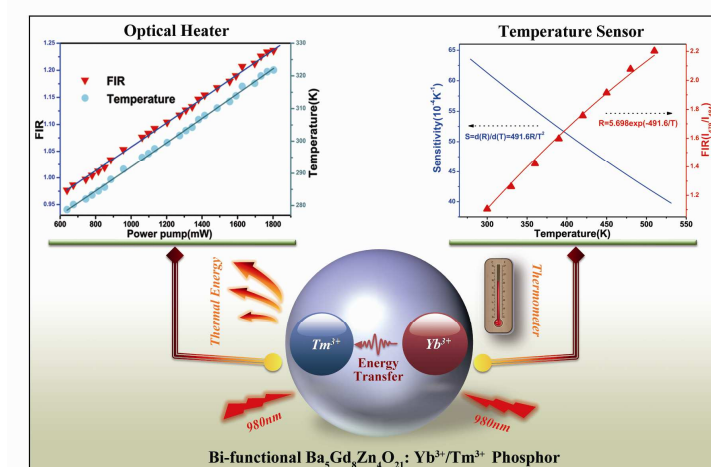


Fig.8 The UCL spectra of the blue bands ( ${}^1\text{G}_{4(1)} / {}^1\text{G}_{4(2)} \rightarrow {}^3\text{H}_6$ ) of  $\text{Tm}^{3+}$  with different pumping power. Inset: temperature ( $\bullet$ ) and FIR ( $\blacktriangledown$ ) as a function of laser pump power in  $\text{Ba}_5\text{Gd}_8\text{Zn}_4\text{O}_{21}: \text{Yb}^{3+}/\text{Tm}^{3+}$ .



## Graphic Abstract



Optical temperature sensor and optical heater based on  $\text{Yb}^{3+}/\text{Tm}^{3+}$  co-doped  $\text{Ba}_5\text{Gd}_8\text{Zn}_4\text{O}_{21}$  phosphors.